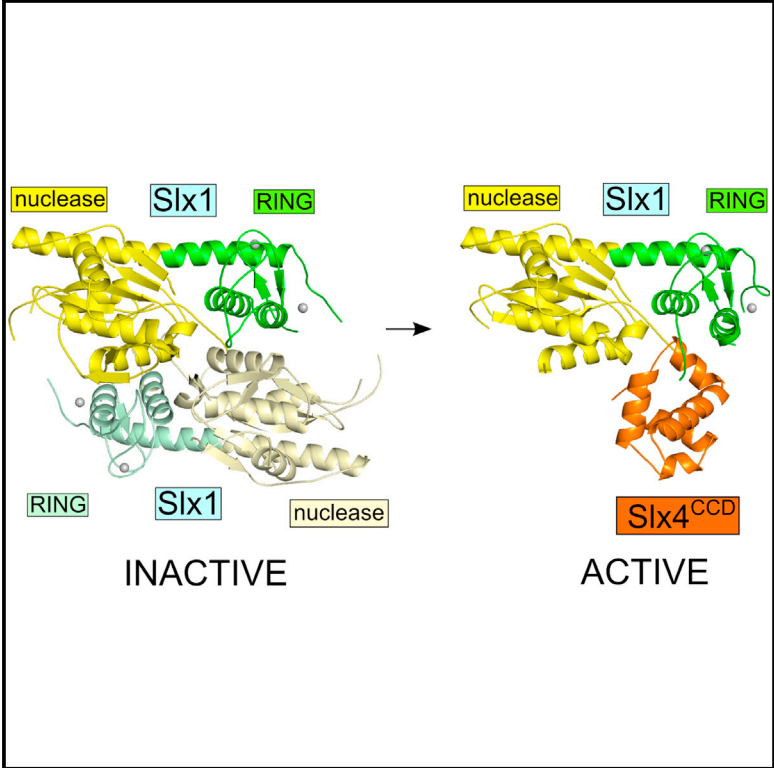


Structural and Mechanistic Analysis of the Slx1-Slx4 Endonuclease

Graphical Abstract



Authors

Vineet Gaur, Haley D.M. Wyatt, ..., Stephen C. West, Marcin Nowotny

Correspondence

mnowotny@iimcb.gov.pl

In Brief

The SLX1-SLX4 endonuclease cleaves branched DNA structures and has critical roles in DNA replication, recombination, and repair. Gaur et al. report structures for yeast Slx1 alone and in complex with the C-terminal domain of Slx4. These studies reveal a potential regulatory mechanism for the nuclease activity of Slx1.

Highlights

- Structural insights into the Slx1 nuclease and Slx1-Slx4 heterodimer
- Slx1 forms a stable homodimer in which the active site is blocked
- Slx1 homodimerization and interaction with Slx4 are mutually exclusive
- Conversion of Slx1 homodimer to Slx1-Slx4 heterodimer is proposed to activate Slx1

Accession Numbers

4XM5
4XLG



Structural and Mechanistic Analysis of the Slx1-Slx4 Endonuclease

Vineet Gaur,¹ Haley D.M. Wyatt,² Weronika Komorowska,¹ Roman H. Szczepanowski,³ Daniele de Sanctis,⁴ Karolina M. Gorecka,¹ Stephen C. West,² and Marcin Nowotny^{1,*}

¹Laboratory of Protein Structure, International Institute of Molecular and Cell Biology, 4 Księcia Trojdena Street, 02-109 Warsaw, Poland

²London Research Institute, Cancer Research UK, Clare Hall Laboratories, Blanche Lane, South Mimms, Herts EN6 3LD, UK

³Biophysics Core Facility, International Institute of Molecular and Cell Biology, 4 Księcia Trojdena Street, 02-109 Warsaw, Poland

⁴European Synchrotron Radiation Facility (ESRF), 71 Avenue des Martyrs, CS 40220, 38043 Grenoble Cédex 9, France

*Correspondence: mnowotny@iimcb.gov.pl

<http://dx.doi.org/10.1016/j.celrep.2015.02.019>

This is an open access article under the CC BY-NC-ND license (<http://creativecommons.org/licenses/by-nc-nd/3.0/>).

SUMMARY

The SLX1-SLX4 endonuclease required for homologous recombination and DNA repair in eukaryotic cells cleaves a variety of branched DNA structures. The nuclease subunit SLX1 is activated by association with a scaffolding protein SLX4. At the present time, little is known about the structure of SLX1-SLX4 or its mechanism of action. Here, we report the structural insights into SLX1-SLX4 by detailing the crystal structure of *Candida glabrata* (*Cg*) Slx1 alone and in combination with the C-terminal region of Slx4. The structure of Slx1 reveals a compact arrangement of the GIY-YIG nuclease and RING domains, which is reinforced by a long α helix. Slx1 forms a stable homodimer that blocks its active site. Slx1-Slx4 interaction is mutually exclusive with Slx1 homodimerization, suggesting a mechanism for Slx1 activation by Slx4.

INTRODUCTION

The human SLX1-SLX4 structure-selective endonuclease plays a key role in DNA repair, homologous recombination, replication fork restart, and telomere maintenance (Svendsen and Harper, 2010). The genes encoding *Saccharomyces cerevisiae* Slx1 and Slx4 were discovered in a genetic screen for mutations that are synthetic lethal in the absence of the Sgs1 helicase, a protein that is important for genome stability (Mullen et al., 2001). Homology searches subsequently identified the *SLX1* and *SLX4* genes in higher eukaryotes (Andersen et al., 2009; Fekairi et al., 2009; Muñoz et al., 2009; Svendsen et al., 2009). Slx1 is an evolutionarily conserved protein that contains an N-terminal GIY-YIG nuclease domain (also called URI domain) and a C-terminal zinc-finger domain. GIY-YIG domains also are present in homing nucleases, the bacterial nucleotide excision-repair nuclease UvrC, and several type II restriction enzymes (Dunin-Horkawicz et al., 2006). The mechanism of substrate binding and cleavage for GIY-YIG family members has been elucidated by crystallographic studies of protein-DNA com-

plexes obtained for two restrictases, namely R.Eco29kl (Mak et al., 2010) and Hpy188I (Sokolowska et al., 2011).

The Slx4 subunit of the Slx1-Slx4 nuclease is thought to provide a scaffold that coordinates the actions of a number of proteins involved in DNA processing (Cybulski and Howlett, 2011). For example, vertebrate SLX4 is a large, multi-domain protein that interacts with several DNA repair proteins (Andersen et al., 2009; Fekairi et al., 2009; Muñoz et al., 2009; Salewsky et al., 2012; Svendsen et al., 2009): (1) the N-terminal region of human SLX4 binds the MSH2-MSH3 mismatch-repair complex and XPF-ERCC1 nucleotide excision-repair enzyme; and (2) the C-terminal portion of SLX4 binds the telomeric proteins TRF2 and RAP1, the PLK1 kinase, and the MUS81-EME1 endonuclease. In all organisms studied to date, SLX1 binds to the extreme C-terminal region of SLX4, which contains an evolutionarily conserved helix-turn-helix motif. Interestingly, in vitro studies have shown that SLX4 stimulates the endonuclease activities of SLX1, MUS81-EME1, and XPF-ERCC1 (Hodskinson et al., 2014; Muñoz et al., 2009; Wyatt et al., 2013). The importance of SLX4 is demonstrated by the observation that biallelic mutations in SLX4 (also known as FANCP) are associated with the cancer-prone disorder Fanconi anemia (Bogliolo et al., 2013; Kim et al., 2011; Stoepker et al., 2011).

Although the amino acid sequence of SLX4 is evolutionarily diverse, the C-terminal region of all SLX4 proteins contains a conserved C-terminal domain (CCD) that underpins the interaction with SLX1 and a DNA-binding SAP domain found in many DNA repair proteins (Andersen et al., 2009; Aravind and Koonin, 2000; Fekairi et al., 2009; Muñoz et al., 2009; Svendsen et al., 2009). In yeast, there are few other discernible domains, whereas SLX4 proteins from higher eukaryotes (e.g., worms, flies, and humans) contain one or two copies of a UBZ family zinc-finger domain known as UBZ4; the MEI9^{XPF} interaction like region (MLR); and a Broad-complex, Tramtrack, and Bric-a-brac (BTB) domain (Stogios et al., 2005).

The role of SLX1-SLX4 in DNA repair has been studied extensively (Cybulski and Howlett, 2011; Sarbajna and West, 2014; Wyatt and West, 2014). Although deletion of Slx1 in yeast does not affect the response to DNA damage, it has been shown that Slx1-Slx4 plays a role in maintaining the integrity of ribosomal loci, which contain tandem repeats that frequently lead to replication fork arrest (Coulon et al., 2004). It is possible that

Slx1-Slx4 is involved in the collapse of stalled forks and the resolution of recombination intermediates, such as Holliday junctions (HJs), after fork recapture (Gritenaite et al., 2014). In human cells, transient depletion of SLX4 leads to an increased sensitivity to alkylating and crosslinking agents, indicating the importance of SLX4 for the repair of DNA inter-strand crosslinks (ICLs) and protein-DNA adducts. Depletion of SLX4 also reduces the efficiency of double-strand break repair and leads to genome instability (Garner et al., 2013; Muñoz et al., 2009; Sarbajna et al., 2014; Svendsen et al., 2009; Wechsler et al., 2011). Collectively, these observations indicate that SLX1 and/or SLX4 have relatively well-conserved roles in processing DNA intermediates that arise at stalled or collapsed replication forks, particularly when cells are treated with DNA-damaging agents that interfere with normal replication fork progression.

Purified *S. cerevisiae* Slx1-Slx4 cleaves various DNA substrates in vitro, including splayed-arm structures, model replication forks, 5'-flaps, and HJs (Fricke and Brill, 2003). For the 5'-flap substrates, the major cleavage site lies in the 5' single-stranded arm at the junction between single- and double-stranded DNA. Whereas Slx1 alone possesses weak nuclease activity, the rate is stimulated approximately 500-fold by Slx4. Purified human SLX1-SLX4 exhibits related activities and cleaves 5'-flaps, 3'-flaps, replication forks, and HJs. Of particular interest, SLX1-SLX4 and MUS81-EME1 cooperate during HJ resolution, with SLX1-SLX4 performing the initial nick such that MUS81-EME1 can resolve the nicked HJ without substrate dissociation (Wyatt et al., 2013).

Although there is a significant amount of functional information available for Slx1-Slx4 and its associated proteins, structural and mechanistic insights for this enzyme are lacking. Here we report the crystal structure of the Slx1 nuclease, obtained using *Candida glabrata* Slx1 (*Cg*-Slx1). The protein forms a compact structure with the GIY-YIG nuclease and RING-finger domains interacting with each other, and the structural arrangement is reinforced by a long α helix. We find that *Cg*-Slx1 forms a stable homodimer in the absence of *Cg*-Slx4. Importantly, the crystal structure of *Cg*-Slx1 in complex with *Cg*-Slx4^{CCD}, together with biochemical analyses, demonstrate that *Cg*-Slx1 homodimerization is mutually exclusive with the formation of a *Cg*-Slx1-Slx4^{CCD} heterodimer, revealing a likely regulatory mechanism for Slx1 endonuclease activity.

RESULTS AND DISCUSSION

Overall Structure of *Cg*-Slx1

To obtain structural information for Slx1, we purified *C. glabrata* Slx1 protein (*Cg*-Slx1) alone and in complex with the conserved C-terminal domain of Slx4 (*Cg*-Slx1-Slx4^{CCD}). When the enzymatic activities of *Cg*-Slx1 and *Cg*-Slx1-Slx4^{CCD} were verified using synthetic DNA substrates (for sequences, see Figures S1A and S1B), we found that *Cg*-Slx1 exhibited little or no activity, whereas the *Cg*-Slx1-Slx4^{CCD} complex cleaved a diverse set of branched DNA structures (Figure 1). The observed nuclease activity was inherent to Slx1, as substitution of an invariant residue in the active site (Slx1^{E79Q}) abolished the nuclease activity of *Cg*-Slx1-Slx4^{CCD} (Figure 1B, bottom). We observed that the HJ was the preferred substrate for *Cg*-Slx1-Slx4^{CCD}, followed

by 5'-flap, splayed arm, and 3'-flap DNA structures (Figures 1B [top] and 1C). In contrast, the enzyme failed to cleave gapped, nicked, and double- or single-stranded DNA substrates. A similar substrate preference was reported for full-length yeast (Fricke and Brill, 2003) and human (Wyatt et al., 2013) enzymes, although *Cg*-Slx1-Slx4^{CCD} was comparatively more active on 3'-flaps. Enzyme titration experiments with the 5'-flap substrate revealed that the primary cleavage product, a nicked or gapped DNA duplex, was processed further to generate a shorter DNA duplex (Figure 1A). However, time-course experiments carried out with limiting amounts of protein revealed that the major reaction was a single nick that converted the 5'-flap into a linear duplex (Figure 1B). This is consistent with the inability of *Cg*-Slx1-Slx4^{CCD} to cleave nicked or gapped DNA duplexes when protein is limiting. To gain more insight into the mechanism by which *Cg*-Slx1-Slx4^{CCD} cleaves 5'-flaps, we prepared two different substrates, each ³²P-labeled on a different oligonucleotide (Figures S1C and S1D). Time-course experiments revealed two independent cleavage sites: a primary incision that removed the 5'-flap, and a less efficient incision reaction that removed the duplex arm. Collectively, our results provide additional evidence for the promiscuous nature of Slx1-Slx4, suggesting that this biochemical property has been conserved throughout evolution.

We next obtained crystals of *Cg*-Slx1^{E79Q}, which belonged to the *P*₄₃₂₁ space group, and diffracted X-rays to 2.34 Å resolution. The protein was predicted to contain a zinc finger, so diffraction data were collected at the zinc absorbance peak wavelength (1.280 Å), and the structure was solved by zinc single-wavelength anomalous diffraction (SAD) (Table S1). The asymmetric unit of the crystal contained one Slx1 molecule and the structure was refined to an *R*_{free} of 25.1% (Table S1). Fragments of simulated annealing composite omit electron density maps are presented in Figure S2A. We noted that the loop regions of the zinc-finger domain had higher B factors and less-well-defined electron density maps, indicating the flexibility of this part of the structure.

The *Cg*-Slx1 monomer consists of two distinct domains: (1) an N-terminal GIY-YIG or URI nuclease domain, and (2) a C-terminal zinc-finger domain. In the *Cg*-Slx1 structure, these two domains interact with each other and form an oblong molecule approximately 70 Å long and 30–40 Å wide (Figure 2). The overall structure is reinforced by a long α helix (helix α 6, located between the two domains and comprising residues 176–214) that spans the entire molecule and provides a scaffold for the two domains. The central element of the nuclease domain is a β sheet consisting of five strands arranged β 2- β 1- β 3- β 6- β 7 (numbered in the amino acid sequence, Figure S2C), with strands β 2 and β 3 oriented antiparallel to β 1, β 6, and β 7 (Figure 2). The β sheet is flanked by six helices; short helix α 1 and long helix α 6 are located on one side of the sheet and four helices (α 2- α 5) are positioned on the other side. The α 2- α 5 region also contains a β hairpin formed by strands β 4 and β 5 (Figure 2). Comparisons of *Cg*-Slx1 structure with related GIY-YIG nucleases can be found in the Supplemental Results and in Figures S2D–S2G. The active site of *Cg*-Slx1 is highly conserved with other GIY-YIG nucleases (Figure S2H), and we therefore propose that the catalytic mechanism of Slx1 is identical to that described for Hpy188I (Sokolowska et al., 2011). Details of the organization of the active site and

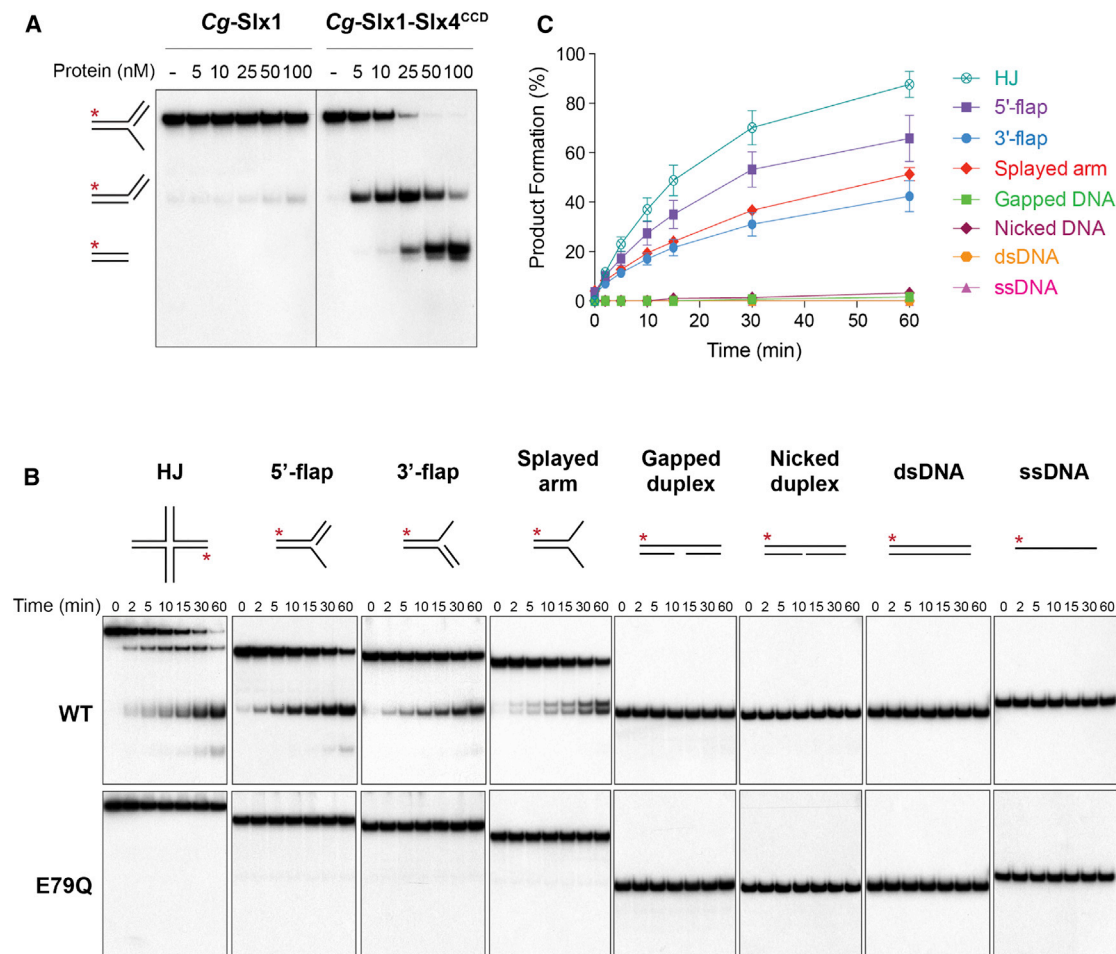


Figure 1. Nuclease Activities of *Cg-Slx1* and *Cg-Slx1-Slx4^{CCD}*

(A) 5'-flap cleavage by *Cg-Slx1* and the *Cg-Slx1-Slx4^{CCD}* complex. 5'-flap DNA (100 nM), spiked with negligible amounts of 5'-³²P-labeled substrate, was incubated with increasing concentrations of *Cg-Slx1* or *Cg-Slx1-Slx4^{CCD}* at 37°C for 15 min. Reaction products were analyzed by native PAGE and autoradiography. Red asterisk, 5'-³²P-labeled oligonucleotide.

(B) Substrate specificity of *Cg-Slx1-Slx4^{CCD}*. The indicated DNA substrates (100 nM), spiked with trace amounts of the corresponding 5'-³²P-labeled substrate, were incubated with 10 nM *Cg-Slx1-Slx4^{CCD}* (top) or 10 nM catalytically inactive *Cg-Slx1^{E79Q}-Slx4^{CCD}* (bottom). At the indicated time points, samples were removed and reaction products were analyzed by native PAGE. Red asterisks, 5'-³²P-labeled oligonucleotides.

(C) Quantification of data shown in (B) by phosphorimaging. Product formation is expressed as a percentage of total radiolabeled DNA. Data are presented as the mean of at least three independent measurements ± SEM.

See also Figure S1.

the catalytic mechanism proposed for *Cg-Slx1* can be found in the Supplemental Results and in Figures S2H and S2I. The C-terminal part of the *Cg-Slx1* structure comprises a zinc-finger domain. Our structure shows that it is a RING finger closely related to domains found in ubiquitin ligases (Supplemental Results; Figures S2J–S2L).

Slx1 Dimerization

Inspection of the *Cg-Slx1* crystal packing revealed that a 2-fold crystallographic axis generated a very tight protein dimer, with a total buried surface area of 4,729 Å² (Figure 3A). At the dimer interface, helix α2 of one monomer was positioned snugly in a groove located between the nuclease and RING domains of the other subunit. Notably, the side chain of Arg72, found at

the N terminus of helix α2, was inserted into a pocket on the surface of the other subunit, where it interacted with the backbone carbonyls of Glu3 and Gln5. Another prominent interaction that stabilized the homodimer involved Tyr86 from the Slx1-specific β4–β5 hairpin of one subunit and helix α7 from the RING domain of the other subunit. Contacts were also made between Glu121, Tyr122, and Tyr86 from one subunit and Thr271, Ile272, and Ile273 of the other. Together, these residues formed a network of charged and van der Waals interactions through their side chains. Two symmetrical copies of this part of the interface were located close to each other and formed a continuous zipper of interdigitated amino acid side chains (Figure 3B).

The extensive dimerization contacts and large buried surface area prompted us to investigate whether *Cg-Slx1* dimerization

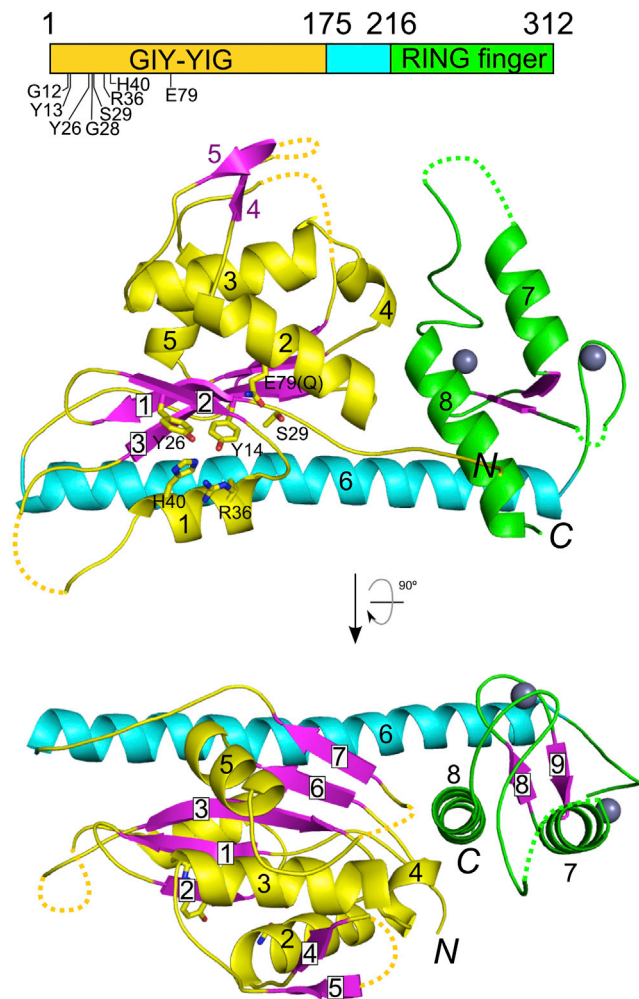


Figure 2. Overall Structure of *Cg*-Slx1

The GIY-YIG nuclease domain is shown in purple for β strands and yellow for the rest of the sequence. The RING domain is shown in green and the connecting scaffold helix $\alpha 6$ in cyan. Zinc ions are shown as gray spheres. The residues forming the active site are shown as sticks and labeled. Dotted lines indicate the loop regions, which were not observed in the electron density maps. Domain boundaries are schematically shown as rectangles on top of the panels with the residue numbers given and active site residues indicated. See also Table S1 and Figure S2.

occurs in solution. To do this, we used gel filtration coupled to multi-angle light scattering (GF-MALS) (Figure 3C) and analytical ultracentrifugation (AUC) (Figure S3A). The molecular weight (MW) of *Cg*-Slx1 measured by GF-MALS was 80.3 kDa and 72.0 kDa by AUC, suggesting that *Cg*-Slx1 exists as a homodimer in solution (calculated MW of 72.0 kDa). We subsequently investigated the multimeric state of the *Cg*-Slx1-Slx4^{CCD} complex. First, we used GF-MALS to determine that the MW of *Cg*-Slx4^{CCD} alone was 19.0 kDa. This is in agreement with the theoretical MW of 19.7 kDa and indicates that *Cg*-Slx4^{CCD} is monomeric in solution. For *Cg*-Slx1-Slx4^{CCD}, the measured MW was 57.0 kDa (GF-MALS) and 47.0 kDa (AUC). Importantly, these data indicate that the *Cg*-Slx1-Slx4^{CCD} complex contains

one molecule of Slx1 and one molecule of Slx4^{CCD} (calculated MW of 57.0 kDa). Our results therefore demonstrate that *Cg*-Slx1 alone exists as a stable homodimer, but, in the presence of *Cg*-Slx4^{CCD}, interacts with this subunit to form a stable heterodimeric complex. Close inspection of the *Cg*-Slx1 homodimeric structure showed that the active site of each subunit was partially blocked by the RING domain of the other subunit (Figures 3A and S4). This suggests that dimerization blocks the activity of *Cg*-Slx1. Indeed, *Cg*-Slx1 (Figure 1A) as well as the *S. cerevisiae* (Fricke and Brill, 2003) and human (Muñoz et al., 2009) enzymes are inactive in the absence of Slx4.

To gain further insight into the *Cg*-Slx1 homodimerization, we prepared a series of *Cg*-Slx1 variants with substitutions in dimer interface residues. These protein variants were structurally unstable (Supplemental Results; Figures S3A–S3C). Additional gel filtration experiments demonstrated that *Cg*-Slx1 homodimerization and *Cg*-Slx1-Slx4^{CCD} complex formation are mutually exclusive, and the exchange between the two forms can be promoted by high salt concentration (Supplemental Results; Figures S3D and S3E).

In summary, our results show that *Cg*-Slx1 is a homodimer in solution. Furthermore, they indicate that *Cg*-Slx1 dimerization provides a physical block to the active site. Thus, these findings provide a potential mechanism by which Slx1 nuclease activity is inhibited.

A Model for DNA Substrate Binding

The *Cg*-Slx1 structure presented here does not contain a DNA substrate. Nonetheless, *Cg*-Slx1-DNA interactions can be modeled based on the conservation of the active site between Slx1 and GIY-YIG restrictases, for which high-resolution protein-DNA structures are available. To this end, we superimposed the Eco29kl structures (Protein Data Bank [PDB] ID 3NIC [Mak et al., 2010]) on our *Cg*-Slx1 structure, which resulted in a good fit between DNA from the Eco29kl structures and the surface of Slx1. The modeling revealed that *Cg*-Slx1 contains two groups of potential DNA-binding residues, all but one of which are located in the nuclease domain (Figure 4A). The first group (Arg35, Arg38, Gln39, and Gln191) could interact with the non-cleaved DNA strand toward its 5' end from the active site. Based on the polarity of the DNA at the active site, these residues are predicted to contact regions of flap and splayed arm substrates that contain only double-stranded DNA (Figure 4B). Arg35, Arg38, and Gln39 were all located in the vicinity of the phosphate groups of the modeled DNA. Sequence alignment of fungal Slx1 proteins revealed that Arg35 and Gln39 are strictly conserved and Arg38 is partially conserved (Figure S2C). Non-conserved Gln191 was also located in this region but was positioned farther from the substrate in our *Cg*-Slx1-DNA model.

The second group of predicted DNA-binding residues (Arg72, Gln77, His80, and His84) was located on the opposite face of the active site relative to the first group. These residues are predicted to contact the 5' region of the cleaved strand that exists as single-stranded DNA in flap and splayed arm substrates. In the Eco29kl-DNA structure, the straight DNA duplex extended farther away from these residues, suggesting that the single-stranded portion of the splayed arm or 5'-flap substrates must be bent to interact with the protein. Gln77, His80, and His84

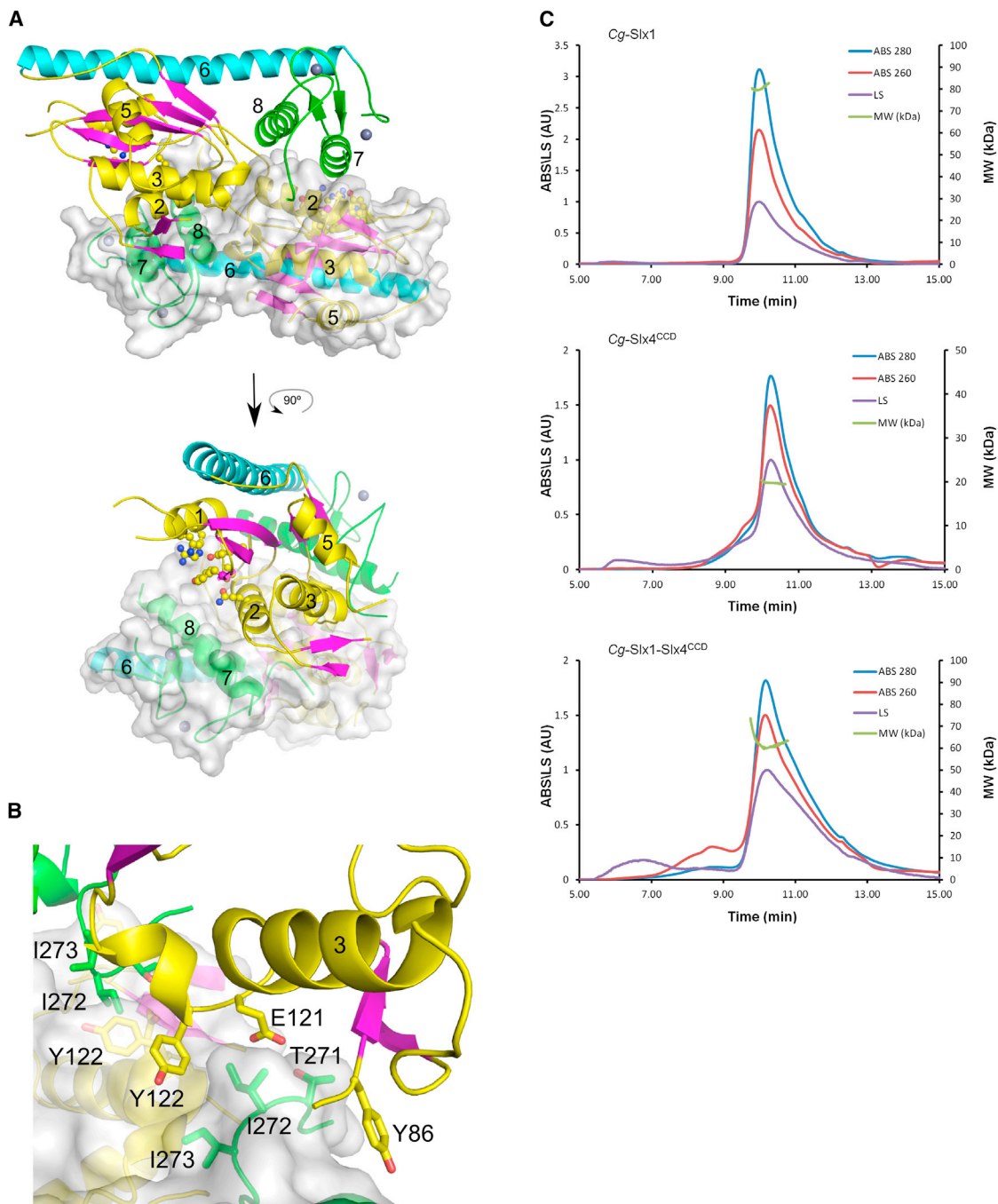


Figure 3. Slx1 Dimerization

(A) One molecule is shown in cartoon representation and colored as in Figure 2. The other subunit is shown in cartoon and transparent surface. The residues forming the active site are shown as ball and sticks.

(B) Close-up of the central region of the dimer interfaces.

(C) Estimation of the MW of Cg-Slx1, Cg-Slx4^{CCD}, and Cg-Slx1-Slx4^{CCD} using GF-MALS. The elution traces from the silica gel filtration column are shown: absorbance at 260 nm (ABS 260) as red trace, at 280 nm (ABS 280) as blue trace, and light scattering (LS) as violet trace. The measured MW throughout the peak is plotted in green (MW values are on the right axis). See also Figure S3.

were all located in helix $\alpha 2$ very close to the metal-coordinating active site residue Glu79. Among fungal Slx1 proteins, Gln77 is conserved and, in some species, replaced with a lysine. Notably,

His80 and His84 are less conserved. Although His80 is substituted by a tryptophan in most species, His84 is always replaced with a charged residue. Interestingly, both Arg72 and the

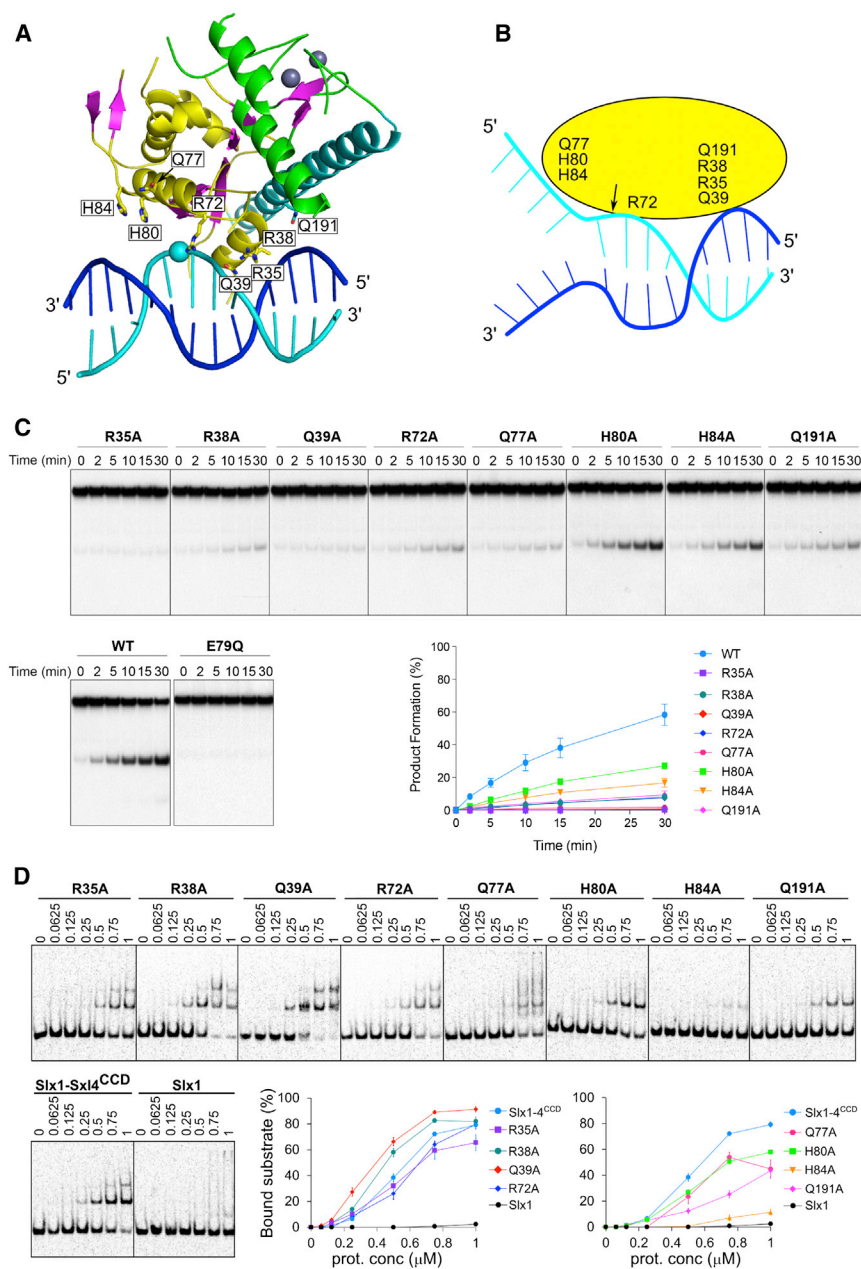


Figure 4. Model of *Cg*-Slx1-DNA Interactions

(A) A view presenting modeled DNA (cyan for the cleaved strand and blue for the non-cleaved one) interacting with *Cg*-Slx1. DNA was modeled by superimposing the catalytic cores of *Cg*-Slx1 and Eco29kI (PDB ID 3NIC [Mak et al., 2010]). The color scheme of *Cg*-Slx1 is the same as in Figure 2. Amino acids predicted to interact with the DNA substrate are shown as sticks. The sphere indicates the scissile phosphate.

(B) Cartoon of the predicted protein-DNA interactions. The site of nucleolytic cleavage is indicated with an arrow.

(C) Cleavage of 5'-flap substrates by *Cg*-Slx1-Slx4^{CCD} mutants that contain single alanine substitutions of residues predicted to interact with DNA. The wild-type *Cg*-Slx1-Slx4^{CCD} and nuclease-inactive *Cg*-Slx1^{E79Q}-Slx4^{CCD} complexes were used as positive and negative controls, respectively. 5'-flap DNA (100 nM) was spiked with negligible amounts of 5'-³²P-labeled substrate and incubated with the indicated *Cg*-Slx1-Slx4^{CCD} complex (10 nM) at 37°C for 0, 2, 5, 10, 15, or 30 min. Reaction products were analyzed by native PAGE. Cleavage products were quantified by phosphorimaging and plotted as the percentage of total radiolabelled DNA. Data are presented as the mean of three independent experiments ± SEM.

(D) DNA binding of *Cg*-Slx1 and *Cg*-Slx1-Slx4^{CCD} (wild-type and mutants) determined by EMSA. Protein, as indicated on the top (μM), was added to 5'-flap substrate (20 nM 5'-³²P-labeled DNA and 105 nM cold DNA). The mixtures were resolved on 6% native TBE gels and visualization by autoradiography. The plots show the percentage of bound substrate. Data are presented as the mean of three independent experiments ± SEM. See also Figure S4.

region around His80 are buried in the *Cg*-Slx1 homodimer, which likely contributes to its inhibition (Figure S4A).

To verify the importance of the potential DNA-binding residues identified in our model, we prepared several *Cg*-Slx1 variants in which these residues were individually substituted with alanine. The *Cg*-Slx1 mutants were purified in the context of the *Cg*-Slx1-Slx4^{CCD} complex and enzyme activity was determined using the 5'-flap substrate (Figure 4C). These mutants showed either a complete loss of nuclease activity (R35A and Q39A) or substantially impaired activity (R38A, R72A, Q77A, Q191A, H80, and H84). We also tested the ability of these Slx1 variants to bind the 5'-flap substrate using electrophoretic mobility shift assays (EMSAs) (Figure 4D). *Cg*-Slx1 alone did not exhibit

DNA-binding properties, while *Cg*-Slx1-Slx4^{CCD} formed a protein-DNA complex with reduced mobility. At high protein concentrations, two protein-DNA complexes were observed, possibly indicating the binding of two Slx1 molecules to DNA. The R38A and Q39A mutants showed slightly stronger substrate binding compared to the wild-type protein, despite exhibiting severe catalytic defects. Importantly, Arg38 and Gln39 are located close to the active site and Gln39 forms a hydrogen bond with active site residue Arg36. Therefore, Arg38 and Gln39 likely participate in active site stabilization upon DNA binding. The R72A variant displayed nearly wild-type binding affinity for the substrate. Its greatly reduced activity suggests that Arg72, which is located in the vicinity of the scissile phosphate, has a more important role in aligning the substrate for cleavage than enhancing substrate affinity. The remaining mutants, namely R35A, Q77A, H80A, H84A, and Q191A, all displayed defects in DNA binding. Interestingly, the most severe defects were observed with the H84A variant.

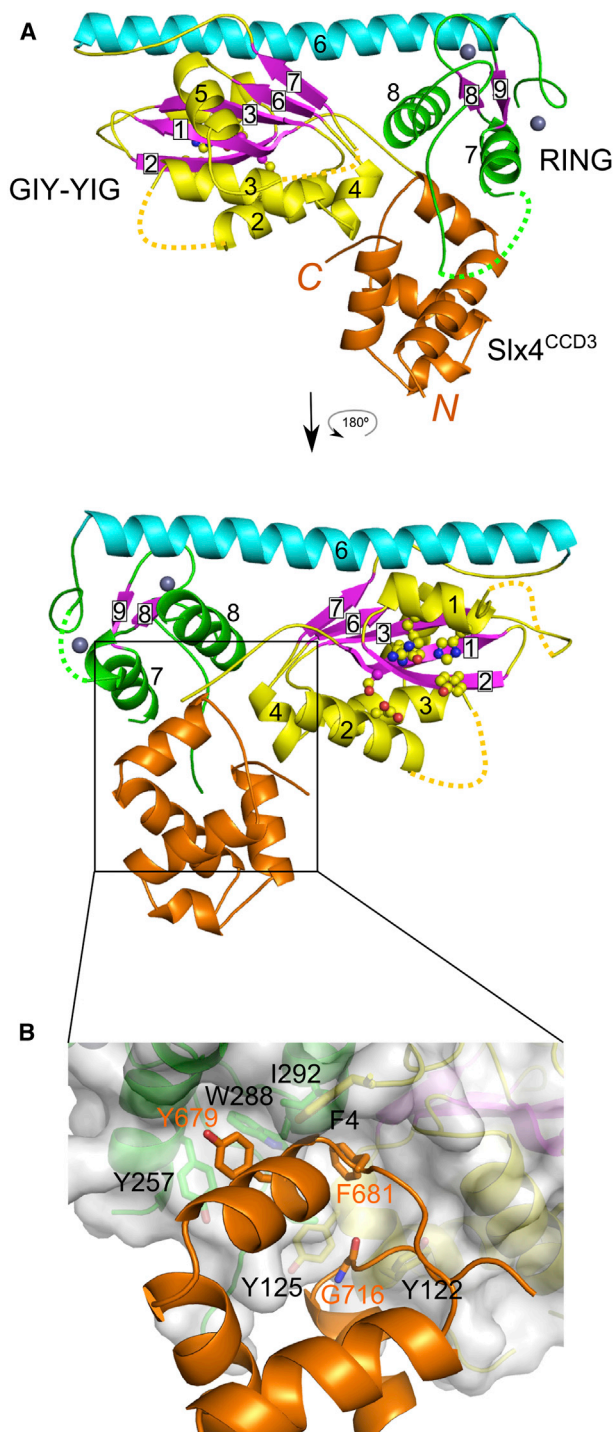


Figure 5. Structure of *Cg*-Slx1-Slx4^{CCD3} Complex

(A) Two views of the complex structure. *Cg*-Slx1 is colored as in Figure 2 and *Cg*-Slx4^{CCD3} is shown in orange. The residues forming the active site are shown as ball and sticks. Dotted lines indicate the loop regions, which were not observed in the electron density maps.

(B) Close-up view of the interactions that occur within the *Cg*-Slx1-Slx4^{CCD3} complex. Selected residues from the interface, including Gly716 from the C terminus of the last helix of CCD3, are shown as sticks.

See also Figure S5.

His84 is located in helix $\alpha 2$, which we postulate to participate in binding the single-stranded portion of the 5'-flap DNA. This result further underscores the importance of helix $\alpha 2$ in the DNA-binding interface.

Collectively, the biochemical results support our proposed model of Slx1-DNA interactions. We have therefore identified two regions of *Cg*-Slx1 that are important for protein-DNA interactions: (1) one predicted to bind double-stranded portion of the DNA, and (2) the other potentially interacting with the single-stranded flap.

Slx1-Slx4^{CCD3} Complex Structure

Our initial crystallization trials with *Cg*-Slx1-Slx4^{CCD} did not yield any crystals, so to gain further insight into *Cg*-Slx1-Slx4 interaction, we performed additional deletion studies. Based on bioinformatic predictions and limited proteolysis experiments, we designed four truncated forms of Slx4^{CCD}, comprising residues 557–685 (*Cg*-Slx4^{CCD1}), 608–685 (*Cg*-Slx4^{CCD1A}), 557–698 (*Cg*-Slx4^{CCD2}), or 647–726 (*Cg*-Slx4^{CCD3}) (Figure S5A). All of these fragments were soluble when expressed in *Escherichia coli* (Figure S5B), but only the CCD3 variant co-purified with *Cg*-Slx1 (Figures S5C and S5D). When we analyzed the activity of *Cg*-Slx1-Slx4^{CCD3} on the 5'-flap DNA, we found that it displayed slightly less activity than *Cg*-Slx1-Slx4^{CCD} and that the cleavage sites for both CCD variants were similar (Figure S5E).

We subsequently obtained crystals of the *Cg*-Slx1-Slx4^{CCD3} complex. They belonged to the $P6_3$ space group and diffracted X-rays to 1.8 Å (Table S1). The structure was solved by molecular replacement using the *Cg*-Slx1 model and the structure of *Cg*-Slx4^{CCD3} was traced manually (Figures 5 and S2B). The overall conformation of *Cg*-Slx1 domains did not change significantly upon Slx4 binding, although the location of the RING domain changed slightly (Figures S5F and S5G). When *Cg*-Slx1 and *Cg*-Slx1-Slx4^{CCD3} were superimposed using the GIY-YIG domains, the position of the RING domain residues differed by up to ~ 3.5 Å. The $\beta 4$ - $\beta 5$ hairpin was not formed in the *Cg*-Slx1-Slx4^{CCD3} complex and this part of the structure adopted a different conformation (Figure 5A). This suggests that the hairpin was stabilized by *Cg*-Slx1 homodimerization.

The structure of *Cg*-Slx4^{CCD3} comprises five α helices. Its closest structural homologs are FF domains mediating protein-protein interactions (Bedford and Leder, 1999). For example, Prp40 FF1 domain (PDB ID 2B7E [Gasch et al., 2006]) can be superimposed on *Cg*-Slx4^{CCD3} with an rmsd of 1.6 Å over 37 C α atoms. Notably, however, the characteristic phenylalanine residues of the FF domain are not conserved in *Cg*-Slx4. *Cg*-Slx4^{CCD3} was positioned in a cleft between the nuclease and RING domains, and most of the interactions between the *Cg*-Slx1 and *Cg*-Slx4^{CCD3} occurred through hydrophobic contacts (Figure 5B). In particular, the second short α helix of *Cg*-Slx4^{CCD3} was placed snugly in a hydrophobic groove on the *Cg*-Slx1 surface. The groove lined up with the side chains of *Cg*-Slx1 Phe4 (nuclease domain) and Tyr257, Ile292, and Ile273 (RING domain). The side chain of *Cg*-Slx4 Phe681, which is conserved in most fungal Slx4 sequences (Figure S5A) and is located in the second short α helix, was inserted into a pocket on the *Cg*-Slx1 surface. The hydrophobic interactions were reinforced further by stacking of *Cg*-Slx1 Tyr257 with

Cg-Slx4 Tyr679. In addition, the backbone carbonyl of this tyrosine formed a hydrogen bond with the N ϵ 1 of the conserved Trp288 in Cg-Slx1. Additional residues at the Cg-Slx1-Slx4 interface included Cg-Slx1 Ile73, Tyr122, and Tyr125, all of which interacted with the C terminus of the last α helix of Cg-Slx4^{CCD3} and the following loop (residues 714–720). The importance of the latter interaction was confirmed by the lack of binding between Cg-Slx1 and Slx4^{CCD2}, in which the C-terminal helix of the CCD is absent.

In murine SLX4, the C1536R mutation abolished its interaction with SLX1 (Castor et al., 2013). This cysteine corresponds to Cg-Slx4 Gly716 located at the C terminus of the last helix of Cg-Slx4^{CCD3}. Insertion in this position of an arginine residue with a large side chain would lead to steric clashes with Cg-Slx1, explaining the effect of C1536R mutation. This observation further validates the interactions identified in our Cg-Slx1-Slx4^{CCD3} structure. Importantly, the position of Cg-Slx4^{CCD3} in the Slx1-Slx4 heterodimer overlapped with the position of one of the Slx1 monomers in the Cg-Slx1 homodimer (Figures S5F and S5G). In fact, several residues, including Cg-Slx1 Tyr122 and Ile273, participated in both Cg-Slx1 homodimerization and Cg-Slx1-Slx4 heterodimerization, thus explaining why the formation of Cg-Slx1 homodimeric and Cg-Slx1-Slx4^{CCD} heterodimeric complexes are mutually exclusive events. Slx4^{CCD3} was located away from the predicted DNA-binding interface of Cg-Slx1 and is not expected to form contacts with the substrate (Figure S4B).

In conclusion, the studies presented here provide the first structural information for Slx1 and its interaction with Slx4. Structure-selective endonucleases pose an inherent threat to genome integrity because broken DNA ends can facilitate chromosome rearrangements and genome alterations that are potentially tumorigenic. It is therefore crucial to keep these endonucleases tightly regulated to ensure cleavage of the correct DNA substrate at an appropriate time in the cell cycle. Recent studies have revealed that these regulatory mechanisms operate at various levels: protein expression (Courcelle et al., 2001), post-translation modification (Mus81-Eme1/Mms4, Yen1) (Blanco et al., 2014; Matos et al., 2011, 2013), nuclear localization (GEN1) (Chan and West, 2014), conformational changes (FEN1) (Kim et al., 2001; Storici et al., 2002), and protein-protein interactions (e.g., XPG, XPF-ERCC1, and SLX-MUS) (Araújo et al., 2001; Li et al., 1994; Wyatt et al., 2013; Zotter et al., 2006). Our data suggest a mechanism of Slx1 regulation through inhibitory homodimerization that would keep Slx1, a promiscuous and potentially dangerous endonuclease, latent and ensure that its activity is tightly regulated in cells.

EXPERIMENTAL PROCEDURES

Crystallization

Purified Cg-Slx1, at a concentration of 10 mg/ml, was subjected to crystallization screens at 18°C using the sitting-drop vapor diffusion method. Prior to crystallization, the protein was dialyzed against buffer containing 20 mM HEPES-NaOH (pH 7.5), 350 mM NaCl, and 1 mM DTT. Crystals were obtained with 1.4 M sodium citrate tribasic dihydrate and 0.1 M HEPES-NaOH (pH 7.5). Crystals were cryoprotected using 30% glycerol (v/v) before data collection. Purified Cg-Slx1-Slx4^{CCD3}, at a concentration of 10 mg/ml, was subjected to crystallization screens at room temperature using the sitting-drop vapor diffusion method. Prior to crystallization, the protein was dialyzed against buffer

containing 20 mM HEPES-NaOH (pH 7.5), 150 mM NaCl, and 1 mM DTT. Crystals were obtained with 0.2 M magnesium chloride hexahydrate, 0.1 M Bis Tris (pH 6.5), and 25% (v/v) PEG 3350 in the presence of a splayed arm DNA substrate with 15-bp double-stranded portion and 5-nt single-stranded overhangs. Crystals were cryoprotected using 30% glycerol (v/v) before data collection.

Diffraction Data Collection, Structure Solution, and Refinement

X-ray diffraction data for Cg-Slx1 were collected at beamline 14.1 at Berliner Elektronenspeicherring-Gesellschaft für Synchrotronstrahlung (BESSY) (Mueller et al., 2012), and data for Cg-Slx1-Slx4^{CCD3} were collected at beamline ID29 at European Synchrotron Radiation Facility (ESRF). Data for the phasing and refinement of Cg-Slx1 structure were collected at 1.280 Å wavelength. Diffraction data used for refinement of the Cg-Slx1-Slx4^{CCD3} structure were collected at 0.97626 Å. Diffraction data were processed and scaled with XDS (Kabsch, 2010). The statistics of the diffraction data are summarized in Table S1. Phases for Cg-Slx1 were determined using single-wavelength anomalous diffraction in AutoSol module in Phenix (Adams et al., 2010), using data collected at Zn peak wavelength (1.280 Å). Phases for Cg-Slx1-Slx4^{CCD3} were determined by molecular replacement using Phaser-MR module in Phenix (Adams et al., 2010). The structure of Cg-Slx1 was used as the starting model for molecular replacement. Interactive model building was performed in COOT (Emsley et al., 2010) and refinement with Phenix with R-free, calculated with 5% of unique reflections. The structures of Cg-Slx1 and Cg-Slx1-Slx4^{CCD3} were refined with 95.7% and 99.7% residues in the favored region of the Ramachandran plot, respectively. Structure validation was carried out using Molprobit analysis (Chen et al., 2010). Structural analyses, including superpositions, and structural figures were prepared in Pymol (<http://www.pymol.org>). Simulated annealing composite omit maps were calculated in CNS 1.3 (Brünger et al., 1998).

Description of protein purification, oligomeric state analysis, nuclease assays, and EMSA can be found in the Supplemental Experimental Procedures.

ACCESSION NUMBERS

The Protein Data Bank accession numbers for the structures of Cg-Slx1 and Cg-Slx1-Slx4^{CCD3} complex reported in this paper are 4XM5 and 4XLG, respectively.

SUPPLEMENTAL INFORMATION

Supplemental Information includes Supplemental Results, Supplemental Experimental Procedures, five figures, and one table and can be found with this article online at <http://dx.doi.org/10.1016/j.celrep.2015.02.019>.

AUTHOR CONTRIBUTIONS

V.G. and W.K. purified and crystallized the proteins. H.D.M.W. performed nuclease assays. V.G. and D.d.S. collected diffraction data. V.G. and M.N. solved and analyzed the structures. V.G., W.K., and R.H.S. performed biophysical characterization. V.G., W.K., and K.M.G. performed initial cloning and protein production tests. M.N. and S.C.W. supervised the project. V.G., H.D.M.W., S.C.W., and M.N. wrote the manuscript.

ACKNOWLEDGMENTS

We thank Professor Matthias Bochtler for critical reading of the manuscript and I. Ptasiewicz for excellent technical assistance. We would like to thank the staff of beamline 14-1 at Berliner Elektronenspeicherring-Gesellschaft für Synchrotronstrahlung (BESSY) for assistance with data collection. This work was supported by a Wellcome Trust International Senior Research Fellowship to M.N. (098022) and by Cancer Research UK, the European Research Council, and the Jeantet Foundation (to S.C.W.). M.N. is a recipient of the Foundation for Polish Science Ideas for Poland award. The research of M.N. was supported in part by an International Early Career Scientist grant from the Howard Hughes Medical Institute. The research was performed using Centre for

Preclinical Research and Technology (CePT) infrastructure (European Union POIG.02.02.00-14-024/08-00 project).

Received: October 28, 2014

Revised: January 16, 2015

Accepted: February 3, 2015

Published: March 5, 2015

REFERENCES

- Adams, P.D., Afonine, P.V., Bunkóczi, G., Chen, V.B., Davis, I.W., Echols, N., Headd, J.J., Hung, L.W., Kapral, G.J., Grosse-Kunstleve, R.W., et al. (2010). PHENIX: a comprehensive Python-based system for macromolecular structure solution. *Acta Crystallogr. D Biol. Crystallogr.* **66**, 213–221.
- Andersen, S.L., Bergstralh, D.T., Kohl, K.P., LaRocque, J.R., Moore, C.B., and Sekelsky, J. (2009). *Drosophila* MUS312 and the vertebrate ortholog BTBD12 interact with DNA structure-specific endonucleases in DNA repair and recombination. *Mol. Cell* **35**, 128–135.
- Araújo, S.J., Nigg, E.A., and Wood, R.D. (2001). Strong functional interactions of TFIIF with XPC and XPG in human DNA nucleotide excision repair, without a preassembled repairosome. *Mol. Cell Biol.* **21**, 2281–2291.
- Aravind, L., and Koonin, E.V. (2000). SAP - a putative DNA-binding motif involved in chromosomal organization. *Trends Biochem. Sci.* **25**, 112–114.
- Bedford, M.T., and Leder, P. (1999). The FF domain: a novel motif that often accompanies WW domains. *Trends Biochem. Sci.* **24**, 264–265.
- Blanco, M.G., Matos, J., and West, S.C. (2014). Dual control of Yen1 nuclease activity and cellular localization by Cdk and Cdc14 prevents genome instability. *Mol. Cell* **54**, 94–106.
- Bogliolo, M., Schuster, B., Stoepker, C., Derkunt, B., Su, Y., Raams, A., Trujillo, J.P., Minguilón, J., Ramírez, M.J., Pujol, R., et al. (2013). Mutations in ERCC4, encoding the DNA-repair endonuclease XPF, cause Fanconi anemia. *Am. J. Hum. Genet.* **92**, 800–806.
- Brünger, A.T., Adams, P.D., Clore, G.M., DeLano, W.L., Gros, P., Grosse-Kunstleve, R.W., Jiang, J.S., Kuszewski, J., Nilges, M., Pannu, N.S., et al. (1998). Crystallography & NMR system: A new software suite for macromolecular structure determination. *Acta Crystallogr. D Biol. Crystallogr.* **54**, 905–921.
- Castor, D., Nair, N., Déclais, A.C., Lachaud, C., Toth, R., Macartney, T.J., Lilley, D.M., Arthur, J.S., and Rouse, J. (2013). Cooperative control of holliday junction resolution and DNA repair by the SLX1 and MUS81-EME1 nucleases. *Mol. Cell* **52**, 221–233.
- Chan, Y.W., and West, S.C. (2014). Spatial control of the GEN1 Holliday junction resolvase ensures genome stability. *Nat. Commun.* **5**, 4844.
- Chen, V.B., Arendall, W.B., 3rd, Headd, J.J., Keedy, D.A., Immormino, R.M., Kapral, G.J., Murray, L.W., Richardson, J.S., and Richardson, D.C. (2010). MolProbity: all-atom structure validation for macromolecular crystallography. *Acta Crystallogr. D Biol. Crystallogr.* **66**, 12–21.
- Coulon, S., Gaillard, P.H., Chahwan, C., McDonald, W.H., Yates, J.R., 3rd, and Russell, P. (2004). Slx1-Slx4 are subunits of a structure-specific endonuclease that maintains ribosomal DNA in fission yeast. *Mol. Biol. Cell* **15**, 71–80.
- Courcelle, J., Khodursky, A., Peter, B., Brown, P.O., and Hanawalt, P.C. (2001). Comparative gene expression profiles following UV exposure in wild-type and SOS-deficient *Escherichia coli*. *Genetics* **158**, 41–64.
- Cybulski, K.E., and Howlett, N.G. (2011). FANCP/SLX4: a Swiss army knife of DNA interstrand crosslink repair. *Cell Cycle* **10**, 1757–1763.
- Dunin-Horkawicz, S., Feder, M., and Bujnicki, J.M. (2006). Phylogenomic analysis of the GIY-YIG nuclease superfamily. *BMC Genomics* **7**, 98.
- Emsley, P., Lohkamp, B., Scott, W.G., and Cowtan, K. (2010). Features and development of Coot. *Acta Crystallogr. D Biol. Crystallogr.* **66**, 486–501.
- Fekairi, S., Scaglione, S., Chahwan, C., Taylor, E.R., Tissier, A., Coulon, S., Dong, M.Q., Ruse, C., Yates, J.R., 3rd, Russell, P., et al. (2009). Human SLX4 is a Holliday junction resolvase subunit that binds multiple DNA repair/recombination endonucleases. *Cell* **138**, 78–89.
- Fricke, W.M., and Brill, S.J. (2003). Slx1-Slx4 is a second structure-specific endonuclease functionally redundant with Sgs1-Top3. *Genes Dev.* **17**, 1768–1778.
- Garner, E., Kim, Y., Lach, F.P., Kottemann, M.C., and Smogorzewska, A. (2013). Human GEN1 and the SLX4-associated nucleases MUS81 and SLX1 are essential for the resolution of replication-induced Holliday junctions. *Cell Rep.* **5**, 207–215.
- Gasch, A., Wiesner, S., Martin-Malpartida, P., Ramirez-Espain, X., Ruiz, L., and Macias, M.J. (2006). The structure of Prp40 FF1 domain and its interaction with the crn-TPR1 motif of Clf1 gives a new insight into the binding mode of FF domains. *J. Biol. Chem.* **281**, 356–364.
- Gritenaite, D., Princz, L.N., Szakal, B., Bantele, S.C., Wendeler, L., Schilbach, S., Habermann, B.H., Matos, J., Lisby, M., Branzei, D., and Pfander, B. (2014). A cell cycle-regulated Slx4-Dpb11 complex promotes the resolution of DNA repair intermediates linked to stalled replication. *Genes Dev.* **28**, 1604–1619.
- Hodskinson, M.R., Silhan, J., Crossan, G.P., Garaycochea, J.I., Mukherjee, S., Johnson, C.M., Schärer, O.D., and Patel, K.J. (2014). Mouse SLX4 is a tumor suppressor that stimulates the activity of the nuclease XPF-ERCC1 in DNA crosslink repair. *Mol. Cell* **54**, 472–484.
- Kabsch, W. (2010). Xds. *Acta Crystallogr. D Biol. Crystallogr.* **66**, 125–132.
- Kim, C.Y., Park, M.S., and Dyer, R.B. (2001). Human flap endonuclease-1: conformational change upon binding to the flap DNA substrate and location of the Mg²⁺ binding site. *Biochemistry* **40**, 3208–3214.
- Kim, Y., Lach, F.P., Desetty, R., Hanenberg, H., Auerbach, A.D., and Smogorzewska, A. (2011). Mutations of the SLX4 gene in Fanconi anemia. *Nat. Genet.* **43**, 142–146.
- Li, L., Elledge, S.J., Peterson, C.A., Bales, E.S., and Legerski, R.J. (1994). Specific association between the human DNA repair proteins XPA and ERCC1. *Proc. Natl. Acad. Sci. USA* **91**, 5012–5016.
- Mak, A.N., Lambert, A.R., and Stoddard, B.L. (2010). Folding, DNA recognition, and function of GIY-YIG endonucleases: crystal structures of R.Eco29kI. *Structure* **18**, 1321–1331.
- Matos, J., Blanco, M.G., Maslen, S., Skehel, J.M., and West, S.C. (2011). Regulatory control of the resolution of DNA recombination intermediates during meiosis and mitosis. *Cell* **147**, 158–172.
- Matos, J., Blanco, M.G., and West, S.C. (2013). Cell-cycle kinases coordinate the resolution of recombination intermediates with chromosome segregation. *Cell Rep.* **4**, 76–86.
- Mueller, U., Darowski, N., Fuchs, M.R., Förster, R., Hellmig, M., Paithankar, K.S., Pühringer, S., Steffien, M., Zocher, G., and Weiss, M.S. (2012). Facilities for macromolecular crystallography at the Helmholtz-Zentrum Berlin. *J. Synchrotron Radiat.* **19**, 442–449.
- Mullen, J.R., Kaliraman, V., Ibrahim, S.S., and Brill, S.J. (2001). Requirement for three novel protein complexes in the absence of the Sgs1 DNA helicase in *Saccharomyces cerevisiae*. *Genetics* **157**, 103–118.
- Muñoz, I.M., Hain, K., Déclais, A.C., Gardiner, M., Toh, G.W., Sanchez-Pulido, L., Heuckmann, J.M., Toth, R., Macartney, T., Eppink, B., et al. (2009). Coordination of structure-specific nucleases by human SLX4/BTBD12 is required for DNA repair. *Mol. Cell* **35**, 116–127.
- Salewsky, B., Schmiester, M., Schindler, D., Digweed, M., and Demuth, I. (2012). The nuclease hSNM1B/Apollo is linked to the Fanconi anemia pathway via its interaction with FANCP/SLX4. *Hum. Mol. Genet.* **21**, 4948–4956.
- Sarbajna, S., and West, S.C. (2014). Holliday junction processing enzymes as guardians of genome stability. *Trends Biochem. Sci.* **39**, 409–419.
- Sarbajna, S., Davies, D., and West, S.C. (2014). Roles of SLX1-SLX4, MUS81-EME1, and GEN1 in avoiding genome instability and mitotic catastrophe. *Genes Dev.* **28**, 1124–1136.
- Sokolowska, M., Czapinska, H., and Bochtler, M. (2011). Hpy188I-DNA pre- and post-cleavage complexes—snapshots of the GIY-YIG nuclease mediated catalysis. *Nucleic Acids Res.* **39**, 1554–1564.
- Stoepker, C., Hain, K., Schuster, B., Hilhorst-Hofstee, Y., Roomans, M.A., Steltenpool, J., Oostra, A.B., Eirich, K., Korthof, E.T., Nieuwint, A.W., et al.

- (2011). SLX4, a coordinator of structure-specific endonucleases, is mutated in a new Fanconi anemia subtype. *Nat. Genet.* **43**, 138–141.
- Stogios, P.J., Downs, G.S., Jauhal, J.J., Nandra, S.K., and Privé, G.G. (2005). Sequence and structural analysis of BTB domain proteins. *Genome Biol.* **6**, R82.
- Storici, F., Henneke, G., Ferrari, E., Gordenin, D.A., Hübscher, U., and Resnick, M.A. (2002). The flexible loop of human FEN1 endonuclease is required for flap cleavage during DNA replication and repair. *EMBO J.* **21**, 5930–5942.
- Svendsen, J.M., and Harper, J.W. (2010). GEN1/Yen1 and the SLX4 complex: Solutions to the problem of Holliday junction resolution. *Genes Dev.* **24**, 521–536.
- Svendsen, J.M., Smogorzewska, A., Sowa, M.E., O'Connell, B.C., Gygi, S.P., Elledge, S.J., and Harper, J.W. (2009). Mammalian BTBD12/SLX4 assembles a Holliday junction resolvase and is required for DNA repair. *Cell* **138**, 63–77.
- Wechsler, T., Newman, S., and West, S.C. (2011). Aberrant chromosome morphology in human cells defective for Holliday junction resolution. *Nature* **471**, 642–646.
- Wyatt, H.D., and West, S.C. (2014). Holliday junction resolvases. *Cold Spring Harb. Perspect. Biol.* **6**, a023192.
- Wyatt, H.D., Sarbajna, S., Matos, J., and West, S.C. (2013). Coordinated actions of SLX1-SLX4 and MUS81-EME1 for Holliday junction resolution in human cells. *Mol. Cell* **52**, 234–247.
- Zotter, A., Luijsterburg, M.S., Warmerdam, D.O., Ibrahim, S., Nigg, A., van Cappellen, W.A., Hoeijmakers, J.H., van Driel, R., Vermeulen, W., and Houtsmuller, A.B. (2006). Recruitment of the nucleotide excision repair endonuclease XPG to sites of UV-induced dna damage depends on functional TFIIH. *Mol. Cell. Biol.* **26**, 8868–8879.